

Cubic anvil cell apparatus for high-pressure and low-temperature physical property measurements

Jin-Guang Cheng(程金光), Bo-Sen Wang(王铂森), Jian-Ping Sun(孙建平), Yoshiya Uwatoko

Citation: Chin. Phys. B . 2018, 27(7): 077403. **doi:** 10.1088/1674-1056/27/7/077403

Journal homepage: http://cpb.iphy.ac.cn; http://iopscience.iop.org/cpb

What follows is a list of articles you may be interested in

Advanced high-pressure transport measurement system integrated with low temperature and magnetic field

Jing Guo(郭静), Qi Wu(吴奇), Liling Sun(孙力玲)

Chin. Phys. B . 2018, 27(7): 077402. **doi:** 10.1088/1674-1056/27/7/077402

Electronic structure and magnetic properties of rare-earth perovskite gallates from first principles

A Dahani, H Alamri, B Merabet, A Zaoui, S Kacimi, A Boukortt, M Bejar

Chin. Phys. B . 2017, 26(1): 017101. **doi:** 10.1088/1674-1056/26/1/017101

Implementation of LDA+Gutzwiller with Newton's method

Jian Zhang(张健), Ming-Feng Tian(田明锋), Guang-Xi Jin(金光希), Yuan-Feng Xu(徐远锋), Xi Dai(戴希)

Chin. Phys. B . 2017, 26(1): 017103. **doi:** 10.1088/1674-1056/26/1/017103

Effects of pressure and/or magnetism on superconductivity of δ-MoN single crystal

Miao Bo-Tong, Wang Shan-Min, Kong Pan-Pan, Jin Mei-Ling, Feng Shao-Min, Zhang Si-Jia, Hao Ai-Min, Yu Xiao-Hui, Jin Chang-Qing, Zhao Yu-Sheng

Chin. Phys. B . 2015, 24(1): 017403. **doi:** 10.1088/1674-1056/24/1/017403

Abnormal lattice contraction of plutonium hydrides studied by first-principles calculations

Ao Bing-Yun, Shi Peng, Guo Yong, Gao Tao

Chin. Phys. B . 2013, 22(3): 037103. **doi:** 10.1088/1674-1056/22/3/037103

TOPICAL REVIEW — Synergetic Extreme Condition User Facility: Breakthroughs and opportunities for the research of physical science

Cubic anvil cell apparatus for high-pressure and low-temperature physical property measurements*

Jin-Guang Cheng(程金光)[1,2,†], Bo-Sen Wang(王铂森)[1,2], Jian-Ping Sun(孙建平)[1,2], and Yoshiya Uwatoko[3]

[1] *Beijing National Laboratory for Condensed Matter Physics and Institute of Physics, Chinese Academy of Sciences, Beijing* 100190, *China*

[2] *School of Physical Sciences, University of Chinese Academy of Sciences, Beijing* 100190 , *China*

[3] *Institute for Solid State Physics, University of Tokyo,* 5-1-5 *Kashiwanoha, Kashiwa, Chiba* 277-8581, *Japan*

(Received 22 February 2018; revised manuscript received 7 April 2018; published online 25 June 2018)

We will build a cubic anvil cell (CAC) apparatus for high-pressure and low-temperature physical property measurements in the synergic extreme condition user facility (SECUF). In this article, we first introduce the operating principle, the development history, and the current status of the CAC apparatus, and subsequently describe the design plan and technical targets for the CAC in SECUF. We will demonstrate the unique advantages of CAC, i.e., excellent pressure homogeneity and large hydrostatic pressure capacity, by summarizing our recent research progresses using CAC. Finally, we conclude by providing some perspectives on the applications of CAC in the related research fields.

Keywords: cubic anvil cell, high-pressure measurements, temperature–pressure phase diagram, strongly correlated electron systems

PACS: 74.62.Fj, 71.27.+a, 07.35.+k, 07.20.Mc **DOI:** 10.1088/1674-1056/27/7/077403

1. Introduction

Recently, research interest has grown in condensed matter physics to explore novel emergent phenomena under high-pressure (HP) conditions. One celebrated example is the recent discovery of superconductivity (SC) with a record-high transition temperature of 203 K when pressurizing sulfur hydride to above 150 GPa.[1] The importance of HP is evidenced by the following aspects: first, pressure (P) is one of the fundamental thermodynamic parameters like temperature (T) that control the states of matter. It was predicted that condensed matters would on average undergo five phase transformations upon compression to 100 GPa. As such, the application of HP provides an effective means to access many new states of matter and can thus expand the universe of matters substantially. Next, pressure can effectively reduce the interatomic distances, enlarge the orbital overlap integral, and strengthen the electron transfer, and thus tip the balance of competing interactions in strongly correlated electron systems. In this regard, HP is one of the key tuning parameters to realize the quantum critical point, which has been considered as a universal phenomenon for many difficult problems in modern condensed matter physics.[2] Consequently, the application of HP would allow one to disentangle the key factors governing the physical properties of interest. It can not only give a critical check on some theoretical proposals but also provide important implications for practical applications. For example, the observation of positive pressure effect on the superconducting transition temperature (T_c) would prompt one to further enhance T_c at the ambient pressure via substituting smaller species, or the chemical pressure.[3] With the advances of HP techniques, researchers have thus focused more on *in situ* measurements of physical properties under HP conditions.

As many intriguing phenomena in condensed matter physics typically occur at low temperatures, it is necessary to combine HP techniques with a cryostat and/or magnet. Currently, piston cylinder cell (PCC)[4,5] and diamond anvil cell (DAC)[6,7] are widely used for high-pressure and low-temperature (HPLT) physical property measurements. The PCC can provide an excellent hydrostatic pressure condition and offer a relatively large sample space suitable for various physical property measurements. However, its maximum pressure of $\sim$ 3 GPa is insufficient for many studies pertaining to condensed matters with a bulk modulus on the order of $\sim$ 100 GPa. In contrast, the DAC can reach pressures above 300 GPa, and is exceptionally powerful in combination with synchrotron x-ray-based techniques owing to its transparent character. However, the sample space is very limited, thereby causing it difficult to measure the physical properties that require electrical contacts. Consequently, a solid or no-pressure transmitting medium is typically utilized when mea-

*Project supported by the National Natural Science Foundation of China (Grant No. 11574377), the State Key Development Program for Basic Research of China (Grant Nos. 2018YFA0305700 and 2014CB921500), the Key Research Program of Frontier Sciences of the Chinese Academy of Sciences (Grant No. QYZDB-SSW-SLH013), and the JSPS KAKENHI (Grant No. 15H03681).

†Corresponding author. E-mail: jgcheng@iphy.ac.cn

© 2018 Chinese Physical Society and IOP Publishing Ltd

suring the resistivity with DAC.[8,9] This will inevitably introduce a strong pressure inhomogeneity and shear strain, and thus hides the intrinsic pressure responses.

Among the various HP techniques, the cubic anvil cell (CAC)[10] stands out as an excellent supplementary that can solve the above-mentioned shortcomings of PCC and DAC. It can reach hydrostatic pressures up to 15 GPa with a relatively large sample space exceeding 1 mm^3. Given the merits of excellent pressure homogeneity and large pressure capacity, we will build a CAC apparatus in the synergic extreme condition user facility (SECUF). In Section 2, we first introduce briefly the operation principle, development history, and current status of the CAC apparatus, and subsequently describe our design plan and technical targets for the CAC to be built in the SECUF. In Section 3, we demonstrate the unique advantages of CAC by summarizing our recent research progresses using CAC. Finally, we conclude by presenting some perspectives on the possible applications of CAC in the related research fields.

2. Cubic anvil cell

Because the CAC has to be placed in a cryostat and/or magnet, the design of CAC involves some special requirements. In the following, we describe briefly its operating principle, development history, and current status.

2.1. Operating principle

As illustrated in Fig. 1(a), the core part of the CAC consists of six anvils converging onto a central cubic gasket from three orthogonal directions; the synchronized movement of these six anvils is driven by a pair of guide blocks that convert the applied uniaxial loading force to a three-axis compression.[10] In the center of the cubic gasket (see Fig. 1(b)), the sample of interest is hung by electrical leads in a Teflon capsule filled with a liquid pressure-transmitting medium (PTM). In comparison with the opposed-anvil-type HP devices such as DAC, such a three-axis compression geometry together with the adoption of liquid PTM can ensure an excellent pressure homogeneity inside the Teflon capsule. This is very important to obtain intrinsic pressure responses. Because all PTMs will be solidified under HPLT conditions, we should minimize its influence by warming up the CAC to room temperature before increasing to a higher pressure.

Currently, most CACs employ 4 mm×4 mm square-top anvils and a 6 mm-edge-length cubic gasket together with the Teflon capsule with an outer diameter of 2 mm (see Fig. 1(b)). These dimensions of the anvil/gasket/Teflon capsule have been proven to be reliable in terms of the pressure efficiency and the surviving rate of electrical leads over the past 30 years. Under these conditions mentioned above, the maximum pressure can reach approximately 8 GPa using the tungsten-carbide (WC) anvils.[10]

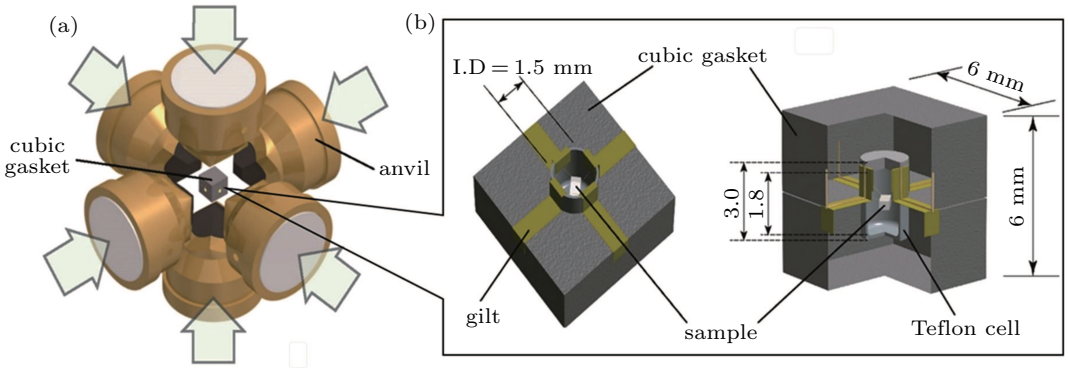


Fig. 1. (color online) (a) Illustration of the operation principle of the CAC in which six anvils converge onto the cubic gasket from three orthogonal directions. (b) Sample configuration in the cubic gasket with the typical dimensions of a gasket and Teflon capsule used for the 4 mm anvils.

2.2. Development history and current status

The CAC apparatus for *in situ* HPLT measurements was originally developed by N. Mori in the 1990s at the Institute for Solid State Physics (ISSP), University of Tokyo. A detailed description of the CAC apparatus can be found elsewhere.[10] As shown in Fig. 2(a), this apparatus is featured by a specially designed top-loading HP cryostat fitted in a 250-ton hydraulic press, which is used to maintain a constant loading force over the CAC device placed inside the cryostat. The low-temperature environment is realized by filling the cryostat with liquid nitrogen and helium, and the lowest temperature of $\sim$ 1.5 K can be achieved using a high-speed vacuum pump. The development of such a CAC apparatus with excellent hydrostatic pressure condition enabled Mori *et al.* to obtain remarkably distinct results from others; for instance, the complete suppression of the Verwey transition around 8 GPa for Fe_3O_4,[11] and the observation of SC at 14.2 K around 7 GPa in β'-(BEDT-FFT)$_2$ICl$_2$.[12] Such CAC apparatus has been successfully operated over 30 years and remains in use in the ISSP and other institutions in Japan.

However, the massive cell body of the conventional CAC apparatus prevents an efficient cooling to well below 2 K and

also renders it difficult to integrate with a strong magnetic field. These issues were overcome by the recent development by Y. Uwatoko using a clamp-type, "palm"-sized CAC.[13] The operation principle is almost identical to the conventional type, except that the applied loading force is locked by tightening the nut of the beryllium-copper clamp cell, which can sustain a maximum loading force of 100 ton for the current design. As illustrated in Figs. 2(c) and 2(d), the weight of the guide block and WC anvil are reduced remarkably to be, respectively, 1/16 and 1/7.5 of the conventional type, albeit the pressure capacity remains nearly unchanged, i.e., ~ 9 GPa for the 4 mm WC anvils. Such a miniature palm CAC has been subsequently integrated with a ^{3}He refrigerator equipped with a five-Tesla magnet (see Fig. 2(b)), thus enabling the combination of multiple extreme conditions including hydrostatic pressures up to ~ 9 GPa, the lowest temperatures down to 0.5 K, and the magnetic field up to 5 T.[14] These developments were crucial for the discovery of pressure-induced heavy-fermion SC in the nonmagnetic quadrupolar system $PrTi_2Al_{20}$ with a maximum $T_c = 1.1$ K at around 9 GPa.[15]

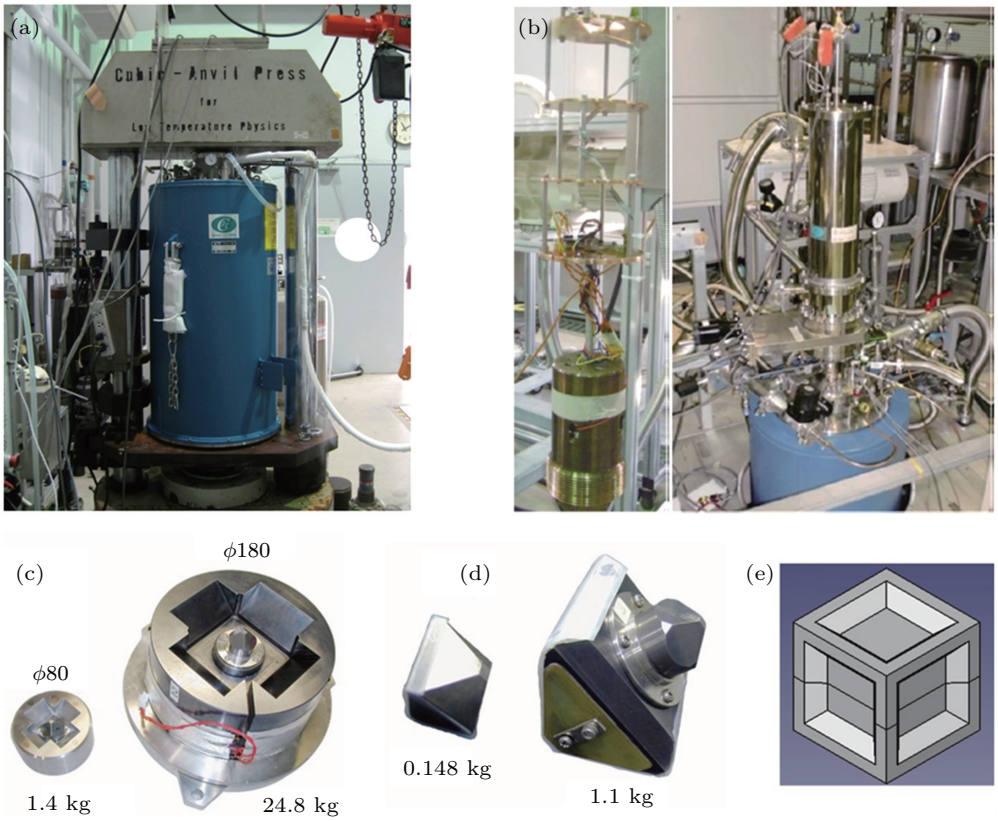


Fig. 2. (color online) (a) Conventional CAC apparatus with a liquid ^{4}He cryostat combined with 250-ton hydraulic press used in the ISSP, University of Tokyo. (b) Palm CAC with a top-loading ^{3}He cryostat used in the ISSP, University of Tokyo, comparison of the (c) guild block and (d) WC anvil for the palm CAC and the conventional CAC. (e) Schematic drawing of the integrated-fin gasket.

To further increase the pressure capacity of the palm CAC, we designed an integrated-fin gasket (see Fig. 2(e)), which shows great improvements in terms of the pressure efficiency and the success rate for the HPLT experiments. By using such a gasket made from MgO and the WC anvils of 2.5-mm square top, we successfully generated pressures over 15 GPa at both room and cryogenic temperatures.[16] Very recently, the palm CAC has been successfully integrated into a cryogen-free dilution refrigerator with a superconducting magnet, achieving the following multiple extreme conditions: $P_{max} = 15$ GPa, $T_{min} = 10$ mK, and $B_{max} = 8$ T, in the ISSP, University of Tokyo. These improvements are indispensable for many unsolved issues in heavy fermion physics.

2.3. CAC to be built in SECUF

Given the excellent pressure homogeneity and large hydrostatic pressure capacity, a CAC apparatus has been approved in the SECUF project. We shall follow the most recent developments of the CAC in the ISSP, University of Tokyo and aim to achieve the state-of-the-art technical targets. We will employ the palm CAC with the integrated-fin gasket and 2.5-mm WC anvils to reach the maximum hydrostatic pressure of 15 GPa. We shall integrate the palm CAC with two different cryostats for different research purposes: (i) a liquid ^{4}He sample-in-vapor cryostat equipped with a 9 T room-temperature (RT) bore cryogen-free superconducting magnet for routine HPLT measurements from RT down to 1.5 K under 9 T; (ii) a cryogen-free ^{3}He/^{4}He dilution refrigerator equipped

with 12 T cold-bore superconducting magnet for ultralow temperature studies. We will perform the following physical property measurements: electrical resistivity, magnetoresistance and Hall resistivity, dielectric constant, ac magnetic susceptibility, and ac specific heat.

3. Recent research progresses with CAC

By taking advantage of the CAC apparatus, we have recently obtained some important results in the research of unconventional SC. In the following, we present three examples to demonstrate the critical role of CAC.

3.1. Discovery of pressure-induced SC in MnP

One of the common features of unconventional superconducting systems such as the heavy-fermion, high-T_c cuprate and iron-pnictide superconductors is that SC emerges on the border of long-range magnetically ordered state. The close proximity of SC to a magnetic instability suggests that the critical spin fluctuations would be crucial for mediating the Cooper pairs. In addition to doping charge carriers, the application of HP is an effective approach for searching novel classes of unconventional superconductors near the magnetic quantum critical point (QCP). After we discovered SC with $T_c \approx 2$ K in CrAs by suppressing its helimagnetic order via the application of hydrostatic pressure of ~ 1 GPa,[17] we explored the pressure-induced SC in MnP by following the similar strategy.[18]

At the ambient pressure, MnP is an itinerant-electron helimagnet with an orthorhombic B31-type structure similar as CrAs. In the absence of magnetic field, MnP undergoes two successive magnetic transitions upon cooling:[19] a transition from the paramagnetic (PM) to ferromagnetic (FM) state at $T_c = 291$ K, and subsequently the second transition to a double helical state at $T_s \approx 50$ K.[19] Earlier HP studies on MnP have revealed that both T_c and T_s decrease with pressure, but the highest hydrostatic pressure of ~ 3 GPa in the previous studies was far from the magnetic QCP.[20]

Figure 3 displays the T–P phase diagram of MnP constructed based on measurements of resistivity and ac magnetic susceptibility up to 11 GPa by using the palm CAC.[18] As shown, both T_s and T_c decrease with pressure and T_s is suppressed completely around 1.4 GPa. Above 3 GPa, the FM transition at T_c changes to a new-type antiferromagnetic (AFM) order marked as T_m, which was later confirmed to be also a helical magnetic order with the propagation vector along the b-axis.[21] Surprisingly, SC emerges below $T_{sc} \approx 1$ K near the critical pressure of $P_c \approx 8$ GPa where the long-range AFM order at T_m just vanishes. Because the majority of the density of states near the Fermi level for MnP is attributed to the Mn-3d states, this discovery renders MnP the first Mn-based superconductor, and the close proximity of SC to a magnetic instability suggests an unconventional pairing mechanism. Moreover, the detailed analysis of the normal-state transport properties evidenced non-Fermi liquid behavior and the dramatic enhancement in the quasiparticles effective mass near P_c associated with the magnetic quantum fluctuations.[18] The discovery of the first Mn-based superconductor dispels the general wisdom about Mn's antagonism to SC and has thus opened a new avenue for investigating more Mn-based superconductors.[22]

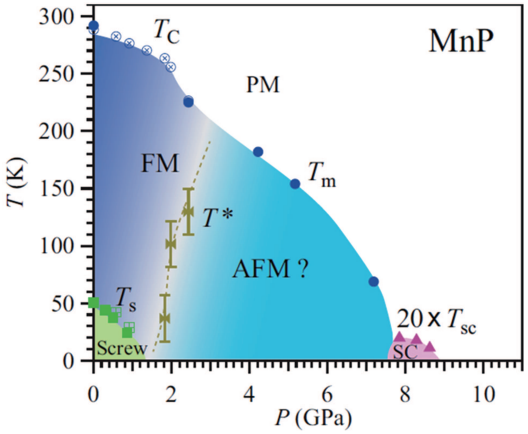


Fig. 3. (color online) T–P phase diagram of MnP. PM: paramagnetic, FM: ferromagnetic, AFM: antiferromagnetic, SC: superconductivity; T_c: PM–FM transition temperature, T_s: FM–Screw transition temperature, T^*: FM–AFM transition temperature, T_m: PM–AFM transition temperature, T_{sc}: superconducting transition temperature. This figure is reproduced from Ref. [18] .

3.2. Dome-shaped magnetic order and high-T_c SC in FeSe under pressure

Among the iron-based superconductors, the structurally simplest β-FeSe and its derived materials have attracted tremendous attention recently owing to its peculiar electronic properties and the great tunability of T_c.[23,24] At the ambient pressure, FeSe undergoes a tetragonal-to-orthorhombic structural transition at $T_s = 90$ K, below which it develops a significant electronic anisotropy or nematicity. Unlike the iron-pnictides superconductors, however, no magnetic order appears within the nematic phase of FeSe, and the SC with $T_c \approx 9$ K occurs without chemical doping or HP. Meanwhile, it was found that HP can induce a static magnetic order at T_m around 1 GPa[25] and promote a high-T_c SC with a T_c of up to 37 K around 7 GPa.[26] These facts render FeSe an ideal platform to study the interplay of SC with magnetism and nematicity.

Despite the extensive HP investigations on FeSe, unfortunately, all previous studies failed to construct a completed T–P phase diagram for FeSe owing to technical limitations; i.e., the PCC with a maximum pressure of ~ 3 GPa is insufficient to reach the highest T_c around 7 GPa,[27] whereas the presence of significant pressure inhomogeneity in the DAC with a solid pressure medium hinders the evolution tracking of the nematic

and magnetic orders.[26] In contrast, the excellent hydrostaticity and large pressure capacity render CAC an ideal choice for this study.

By performing HP resistivity and ac magnetic susceptibility up to 15 GPa with the palm CAC on high-quality FeSe single crystals, we constructed its most comprehensive T–P phase diagram[28] (see Fig. 4), which maps out the explicit evolutions with the pressure of T_s, T_c, and T_m. As shown, we uncovered a previously unknown dome-shaped $T_m(P)$, having two end points situated on the boundaries separating the three plateaus of $T_c(P)$. Our results provide compelling evidence linking intimately the sudden enhancement of T_c to 38 K to the suppression of the long-rang magnetic order. The fact that the optimal T_c is achieved when the long-range antiferromagnetic order just vanishes is reminiscent of the situations shown frequently in the FeAs-based superconductors.

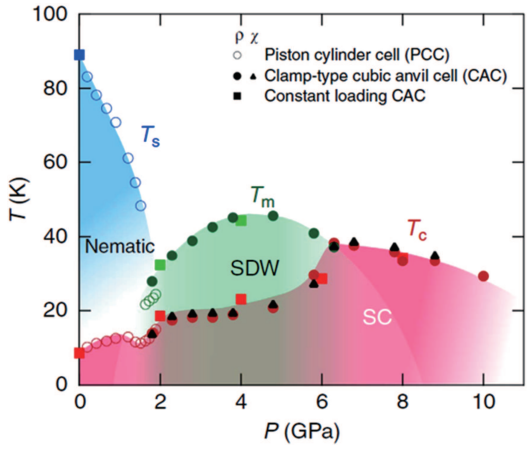


Fig. 4. (color online) T–P phase diagram of FeSe. T_s for the tetragonal to orthorhombic structural transition, T_m for the antiferromagnetic or SDW transition, T_c for the superconducting transition. This figure is reproduced from Ref. [28].

Previous studies on the FeSe-derived high-T_c (> 30 K) superconductors, including $A_xFe_{2-y}Se_2$ (A = K, Cs, Rb, Tl), (Li,Fe)OHFeSe, and monolayer FeSe film, have shown a distinct Fermi surface (FS) topology consisting of only electron pockets near the Fermi level.[23] In contrast, the FS of FeAs-based superconductors typically consists of hole and electron pockets near the Brillouin zone center and corners, respectively. Thus, the distinct FS topology between FeAs- and FeSe-based materials has challenged the current theories on a unified understanding of the mechanism of iron-based superconductors.

In contrast to the electron-doping approaches, the application of HP does not introduce extra electron carriers, yet can still enhance the T_c of bulk FeSe to ~ 38 K near 6 GPa. To understand the mechanism of pressure-induced high-T_c SC in FeSe, it is important to obtain the information about the evolution of FS under HP—a regime in which angle-resolved photoemission spectroscopy experiments are impractical, and where quantum oscillation measurements are challenging. Alternatively, we measured the Hall effect under hydrostatic pressures up to 8.8 GPa with the CAC to gain further insights into the electronic structure evolution of FeSe at HP.[29]

As shown in Fig. 5, our results demonstrate that the electrical transport properties of FeSe at HPs with $T_c^{max} = 38.3$ K are dominated by the hole carriers, which is in contrast with the known FeSe-derived high-T_c superconductors that are typically heavily electron-doped. In addition, we observed an enhancement in the Hall coefficient R_H near the critical pressure where the optimal T_c is realized with a simultaneous suppression of the long-range magnetic order. This implies a strong reconstruction of the FS due to the magnetic order, consistent with the ordering pattern driven by interband scattering. More importantly, our results show a continuous path to high-T_c SC in chalcogenides without electron doping. Our results constitute a significant step forward in presenting a unified picture on the current understanding of iron-based high-T_c superconductors, specifically by demonstrating that high T_c in FeSe can be achieved with an electronic structure and other characteristics similar to the FeAs-based high-T_c superconductors.

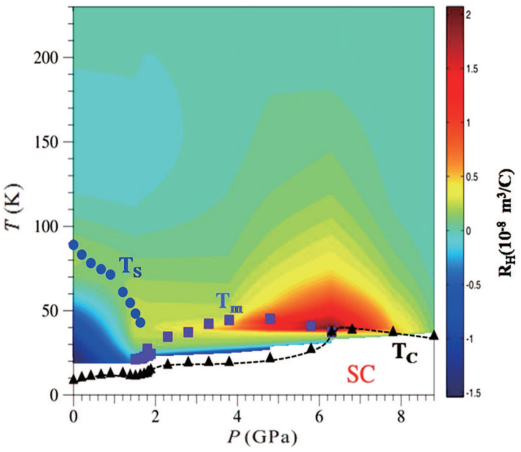


Fig. 5. (color online) T–P phase diagram of FeSe superimposed by a contour plot of Hall coefficient R_H. This figure is reproduced from Ref. [29].

3.3. Reemergence of high-T_c SC in (Li,Fe)OHFeSe under pressure

Although the bulk FeSe displays a relatively low $T_c = 8.5$ K within the nonmagnetic nematic phase below $T_s = 90$ K, a high-T_c SC with T_c above 30–40 K have been successfully achieved via intercalating some alkali–metal ions, ammonia, or organic molecules in between the adjacent FeSe layers, such as in $A_xFe_{2-y}Se_2$ (A = K, Rb, Cs, Tl),[30] $A_x(NH_3)_yFeSe$,[31] and (Li, Fe)OHFeSe.[32] We refer these high-T_c superconductors derived directly from FeSe as the SC-I phase. The superconducting mechanism for these SC-I phases has been subjected to extensive investigations, and the observed common FS topology consisting of only electron pockets in the Brillouin zone corners suggests that the electron doping plays an

essential role for achieving a high T_c, in agreement with the gate-voltage regulation experiments on the FeSe flakes.[33]

Starting from the SC-I phase in $A_xFe_{2-y}Se_2$, it was reported that pressure can induce the sudden reemergence of a second superconducting phase (denoted as SC-II hereafter) with a higher T_c of up to 48.7 K above $\sim$ 10 GPa.[34] A similar SC-II phase has also been observed in $Cs_{0.4}(NH_3)_yFeSe$ under HP.[35] Although the reemergence of the SC-II phase with a higher T_c is intriguing and a different pairing symmetry has been proposed theoretically,[36] the intrinsic superconducting- and normal-state properties have been poorly characterized thus far owing to some sample and technical difficulties. For example, $A_xFe_{2-y}Se_2$ superconductors are prone to phase separation accompanied by the intergrowth of the antiferromagnetic insulating $A_2Fe_4Se_5$ phase. Moreover, HP techniques capable of both large pressure capacity and good hydrostaticity are required to obtain reliable superconducting- and normal-state properties. Therefore, these complexities have hampered the proper understanding of the intriguing SC-II phase of these FeSe-derived materials.

To approach this intriguing problem, we focus on the recently discovered $(Li_{1-x}Fe_x)$OHFeSe,[32] which is free from phase separation, relatively stable in air, and more importantly, can be obtained in high-quality single crystals via a specially designed hydrothermal ion-exchange method.[37] Using the palm CAC, we recently performed detailed magnetotransport measurements on $(Li_{1-x}Fe_x)$OHFeSe single crystals under hydrostatic pressures up to 12.5 GPa.[38]

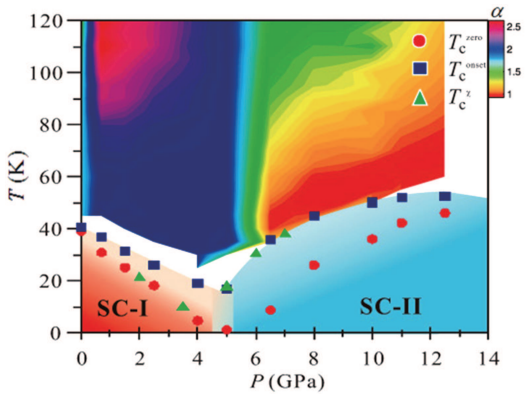


Fig. 6. (color online). T–P phase diagram of (Li,Fe)OHFeSe. SC-I and SC-II represents two distinct superconducting regions. The contour color plot of the normal-state resistivity exponent α illustrates a sharp transition of the normal state from the Fermi liquid for SC-I to the non-Fermi liquid for the SC-II phase. This figure is reproduced from Ref. [38].

The primary results are summarized in Fig. 6. We found that the ambient-pressure SC-I phase is suppressed gradually by increasing pressure to $P_c = 5$ GPa, above which a new SC-II phase with a higher T_c over 50 K emerges gradually. More importantly, our high-precision resistivity data enabled us to uncover a sharp transition of the normal state from a Fermi liquid for SC-I to a non-Fermi liquid for the SC-II phase. In addition, the reemergence of a higher T_c SC-II phase is found to accompany with a concurrent enhancement in the electron carrier density. Such information was unavailable in the previous HP studies on the FeSe-derived high-T_c superconductors.[33,34] The present work thus provides positive correlations between the high-T_c SC in SC-II with an FS reconstruction, which is not induced by a structural transition, as confirmed by our HP structural study.[38]

4. Conclusion and perspectives

In summary, the CAC apparatus has some unique advantages over other HP techniques for low-temperature physical property measurements. First, the three-axis compression geometry together with the sample in liquid medium ensures excellent pressure homogeneity, and thus allows one to obtain the intrinsic pressure effects. Next, the CAC can reach a high hydrostatic pressure up to 15 GPa, which is an important pressure range to alter the ground states of condensed matters having a bulk modulus on the order of 100 GPa. In addition, the sample space of the CAC is relatively large to facilitate the accurate measurements of different physical properties such as resistivity, magnetic susceptibility, and ac specific heat.

Given the excellent hydrostatic pressure condition and large pressure capacity, we plan to build a CAC apparatus in the SECUF project and aim to achieve the state-of-the-art technical targets, i.e., the highest hydrostatic pressure of 15 GPa, the lowest temperature of $<$50 mK, and the strongest magnetic field of 12 T. Under these multiple extreme conditions, we will be able to perform the following measurements: electrical resistivity, magnetoresistance and Hall resistivity, dielectric constant, ac magnetic susceptibility, and ac specific heat.

Upon completion, the CAC apparatus will be open to both domestic and overseas users for collaborative research in different subjects. The CAC is especially useful in the field of strongly correlated electron systems: it can be used to tune the competing interactions to realize different ground states,[39] to explore exotic phenomena such as unconventional SC associated with pressure-induced QCP,[17,18] and to manipulate the metal–insulator transition or other phase transitions.[11,40] In the emergent field of topological materials, the CAC can also be employed to engineer the band gap size or the band topology to access different topological states,[41,42] or even to realize topological phase transitions.[43]

Acknowledgment

The authors would like to thank the following collaborators: Prof. M. Hedo, Prof. K. Matsubayashi, Ms. S. Nagasaki, Mr. W. Wu, Prof. J. L. Luo, Mr. K. Matsuura, Prof. T. Shibauchi, Dr. J. Q. Yan, Dr. P. Shahi, Prof. X. L. Dong, Prof.

Z. X. Zhao, Prof. W. G. Yang, Prof. G. M. Zhang, and Prof. D. J. Singh, for their contributions to the studies listed in this manuscript.

References

[1] Drozdov A P, Eremets M I, Troyan I A, Ksenofontov V and Shylin S I 2015 *Nature* **525** 73
[2] Coleman P and Schofield A J 2005 *Nature* **433** 226
[3] Schilling J S 2002 *NATO Science Series* **48** 345
[4] Walker I R 1999 *Rev. Sci. Instrum.* **70** 3402
[5] Uwatoko Y 2002 *Rev. High Press. Sci. Tech.* **12** 306
[6] Jayaraman A 1983 *Rev. Mod. Phys.* **55** 65
[7] Feng Y J, Silevitch D M and Rosenbaum T F 2014 *Rev. Sci. Instrum.* **85** 033901
[8] Mao H K and Bell P M 1981 *Rev. Sci. Instrum.* **52** 615
[9] Gao C X, Han Y H, Ma Y Z, White A, Liu H W, Lou J F, Li M, He C Y, Hao A M, Huang X W, Pan Y W and Zou G T 2005 *Rev. Sci. Instrum.* **76** 083912
[10] Mori N, Takahashi H and Takeshita N 2004 *High Pressure Research* **24** 225
[11] Mori N, Todo S, Takeshita N, Mori T and Akishige Y 2002 *Physica B* **312** 686
[12] Taniguchi H, Miyashita M, Uchiyama K, Kazuhiko S, Mori N, Okamoto H, Miyagawa K, Kanoda K, Hedo M and Uwatoko Y 2003 *J. Phys. Soc. Jpn.* **72** 468
[13] Uwatoko Y, Matsubayashi K, Matsubayashi K, Aso N, Nishi M, Fujiwara T, Hedo M, Tabata S, Takagi K, Tado M and Kagi H 2008 *Rev. High Press. Sci. Tech.* **18** 230
[14] Matsubayashi K, Hisada A, Kawae T and Uwatoko Y 2012 *Rev. High Press. Sci. Tech.* **22** 206
[15] Matsubayashi K, Tanaka T, Sakai A, Nakatsuji S, Kubo Y and Uwatoko Y 2012 *Phys. Rev. Lett.* **109** 187004
[16] Cheng J G, Matsubayashi K, Nagasaki S, Hisada A, Hirayama T, Hedo M, Kagi H and Uwatoko Y 2014 *Rev. Sci. Instrum.* **85** 093907
[17] Wu W, Cheng J G, Matsubayashi K, Kong P P, Lin F K, Jin C Q, Wang N L, Uwatoko Y and Luo J L 2014 *Nat. Commun.* **5** 5508
[18] Cheng J G, Matsubayashi K, Wu W, Sun J P, Lin F K, Luo J L and Uwatoko Y 2015 *Phys. Rev. Lett.* **114** 117001
[19] Komatsubara T, Shinohara S, Suzuki T and Hirahara E 1969 *J. Appl. Phys.* **40** 1037
[20] Banus M D 1972 *J. Solid State Chem.* **4** 391
[21] Matsuda M, Ye F, Dissanayake S E, Cheng J G, Chi S, Ma J, Zhou H D, Yan J Q, Kasamatsu S, Sugino O, Kato T, Matsubayashi K, Okada T and Uwatoko Y 2016 *Phys. Rev. B* **93** 100405(R)
[22] Norman M R 2015 *Physics* **8** 24
[23] Liu X, Zhao L, He S, He J, Liu D, Mou D, Shen B, Hu Y, Huang J and Zhou X J 2015 *J. Phys.: Condens. Matter* **27** 183201
[24] Wang Q Y, Li Z, Zhang W H, Zhang Z C, Zhang J S, Li W, Ding H, Ou Y B, Deng P, Chang K, Wen J, Song C L, He K, Jia J F, Ji S H, Wang Y Y, Wang L L, Chen X, Ma X C and Xue Q K 2012 *Chin. Phys. Lett.* **29** 037402
[25] Bendele M, Amato A, Conder K, Elender M, Keller H, Klauss H H, Luetkens H, Pomjakushina E, Raselli A and Khasanov R 2010 *Phys. Rev. Lett.* **104** 087003
[26] Medvedev S, McQueen T M, Troyan I A, Palasyuk T, Eremets M I, Cava R J, Naghavi S, Casper F, Ksenofontov V, Wortmann G and Felser C 2009 *Nat. Mater.* **8** 630
[27] Terashima K, Kikugawa N, Kasahara S, Watashige T, Shibauchi T, Matsuda Y, Wolf T, Bohmer A E, Hardy F, Meingast C, Lohneysen H V and Uji S 2015 *J. Phys. Soc. Jpn.* **84** 063701
[28] Sun J P, Matsuura K, Ye G Z, Mizukami Y, Shimozawa M, Matsubayashi K, Yamashita M, Watashige T, Kasahara S, Matsuda Y, Yan J Q, Sales B C, Uwatoko Y, Cheng J G and Shibauchi T 2016 *Nat. Commun.* **7** 12146
[29] Sun J P, Ye G Z, Shahi P, Yan J Q, Matsuura K, Kontani H, Zhang G M, Zhou Q, Sales B C, Shibauchi T, Uwatoko Y, Singh D J and Cheng J G 2017 *Phys. Rev. Lett.* **118** 147004
[30] Guo J G, Wang G, Wang S C, Zhu K X, Zhou T T, He M and Cheng X L 2010 *Phys. Rev. B* **82** 180520(R)
[31] Scheidt E-W, Hathwar V R, Schmitz D, Dunbar A, Scherer W, Mayr F, Tsurkan V, Deisenhofer J and Loidl A 2012 *Eur. Phys. J. B* **85** 279
[32] Lu X F, Wang N Z, Wu H, Wu Y P, Zhao D, Zeng X Z, Lou X G, Wu T, Bao W, Zhang G H, Huang F Q, Huang Q Z and Chen X H 2015 *Nat. Mater.* **14** 325
[33] Lei B, Cui J H, Xiang Z J, Shang C, Wang N Z, Ye G J, Luo X G, Wu T, Sun Z and Chen X H 2016 *Phys. Rev. Lett.* **116** 077002
[34] Sun L L, Chen X J, Guo J, Gao P W, Huang Q Z, Wang H D, Fang M H, Chen X L, Chen G F, Wu Q, C. Z, Gu D C, Dong X L, Wang L, Yang K, Li A G, Dai X, Mao H K and Zhao Z X 2012 *Nature* **483** 67
[35] Izumi M, Zheng L, Sakai Y, Goto H, Sakata M, Nakamoto Y, Nguyen H L T, Kagayama T, Shimizu K, Araki S, Kobayashi T C, Kambe T, Gu D C, Guo J, Liu J, Li Y C, Sun L L, Prassides K and Kubozono Y 2015 *Sci. Rep.* **5** 9477
[36] Das T and Balatsky A V 2013 *New J. Phys.* **15** 093045
[37] Dong X L, Jin K, Yuan D N, Zhou H X, Yuan J, Huang Y L, Hua W, Sun J L, Zheng P, Hu W, Mao Y Y, Ma M W, Zhang G M, Zhou F and Zhao Z X 2015 *Phys. Rev. B* **92** 064515
[38] Sun J P, Shahi P, Zhou H X, Huang Y L, Chen K Y, Wang B S, Ni S L, Li N N, Zhang K, Yang W G, Uwatoko Y, Xing G, Sun J, Singh D J, Jin K, Zhou F, Zhang G M, Dong X L, Zhao Z X and Cheng J G 2018 *Nat. Commun.* **9** 380
[39] Zhou J S, Goodenough J B and Dabrowski B 2005 *Phys. Rev. Lett.* **94** 226602
[40] Li Y, Sun Z, Cai J W, Sun J P, Wang B S, Zhao Z Y, Uwatoko Y, Yan J Q and Cheng J G 2017 *Chin. Phys. Lett.* **34** 087201
[41] Xiang Z J, Ye G J, Shang C, Lei B, Wang N Z, Yang K S, Liu D Y, Meng F B, Lou X G, Zou L J, Sun Z, Zhang Y and Chen X H 2015 *Phys. Rev. Lett.* **115** 186403
[42] Zhang J L, Guo C Y, Zhu X D, Ma L, Zheng G L, Wang Y Q, Pi L, Cheng Y, Yuan H Q and Tian M L 2017 *Phys. Rev. Lett.* **118** 206601
[43] Zhang C, Sun J P, Liu F L, Narayan A, Li N N, Yuan X, Liu Y W, Dai J H, Long Y W, Uwatoko Y, Shen J, Sanvito S, Yang W G, Cheng J G and Xiu F X 2017 *Phys. Rev. B* **96** 155205